SRC TR 88-20

Kinematic Analysis of Tendon-Driven Robotic Mechanisms Using Graph Theory

by

Lung-Wen Tsai and Jyh-Jone Lee

Kinematic Analysis of Tendon-Driven Robotic Mechanisms Using Graph Theory

Lung-Wen Tsai*
Associate Professor

Jyh-Jone Lee
Graduate Research Assistant

Department of Mechanical Engineering
and
Systems Research Center

The University of Maryland
College Park, MD 20742

* Member of ASME

ABSTRACT

The kinematic structure of tendon-driven robotic mechanisms has been investigated with the aid of graph theory. The correspondence between the graph representation of the kinematic structure and the mechanism has been established. We have shown that the kinematic structure of tendon-driven kinematic chains is similar to that of epicyclic gear trains. We have also shown that, using the concept of fundamental circuit, displacement equations of tendon-driven robotic mechanisms can be systematically derived from the kinematic structure. The theory has been demonstrated by the kinematic analysis of three articulated robotic devices.

To be submitted to the 1988 ASME Mechanisms Conference for presentation and publication.

1. Introduction

The kinematic structure of a robot manipulator often takes the form of an open-loop kinematic chain. An open-loop manipulator is mechanically simple and easy to construct. However, it does require the actuators to be located along the joint axes which, in turn, increases the inertia of the manipulator system. In order to reduce the inertia load, partially closed-loop kinematic chains have been designed. For example, the Cincinnati Milacron T^3 robot uses a three-DOF (Degree-of-Freedom) bevel-gear-train for its wrist mechanism so that the wrist actuators can be installed remotely from the wrist [14].

Another method of reducing the inertia is to use tendon or belt for force transmission. A tendon- or belt-driven articulated manipulator has the advantage of remote control. A few tendon-driven mechanical systems can be found in the literature [8-13]. To date, the kinematic or static analysis of such mechanical systems has been accomplished on a one-by-one basis. The purpose of this investigation is to establish a systematic procedure for the kinematic and static analysis of multi-degree-of-freedom, tendon-driven, robotic mechanisms.

The application of graph theory to the kinematic analysis and synthesis of epicyclic gear trains has been well established in recent years [1-3, 5-7, 15-16]. In what follows, we will investigate the kinematic structure of tendon-driven robotic mechanisms using graph representation. We will demonstrate that the kinematic structure of tendon-driven mechanisms is in every way similar to that of epicyclic gear trains. Therefore, the fundamental circuit equation developed for the kinematic analysis of epicyclic gear

trains [16] can be directly applied to this type of mechanisms. We will also demonstrate that once the displacement equations are obtained, the input and output torque (or forces) relationship can be easily derived.

2. General Assumptions

Gear trains are commonly used to transmit power or motion between either parallel or non-parallel shafts with small offset distance. When the center distance between two offset shafts becomes large, it is often necessary to add intermediate shafts and idler gears in order to keep the size of the gears reasonably small.

An alternative method of power transmission is to use tendons or belts and pulleys. We shall call this type of mechanisms tendon-driven mechanisms. In what follows, we shall consider only those mechanisms which obey the following assumptions:

(i) The tendons are always under tension and the amount of stretch in tendons due to variation of tension is negligible.

(ii) The friction between pulleys and tendons is large enough to prevent relative sliding to occur.

(iii) The mechanism shall obey the general DOF equation, i.e., no special proportions are required to ensure the mobility of a tendon-driven mechanism.

(iv) Each pulley must have a turning pair on its axis and every pair of pulleys connected by a tendon must have a carrier (or arm) in order to maintain a constant center distance between the pulleys.

(v) The mechanism shall be of articulated type, i.e., after the removal of tendons and pulleys, the mechanism becomes an open-loop chain.

3. Structural Representations

(a) Functional Representation. This refers to the conventional drawing of a mechanism. Shafts, pulleys, tendons, and other elements are identified as such. For the reason of clarity and simplicity, only functional elements essential to the kinematic structure are shown. Different functional representation may represent different designs of the same topological structure (e.g., planar vs. spatial mechanisms). For tendon-driven robotic mechanisms, there are two basic routing techniques. The first is known as the open-ended tendons and the second the endless tendons.

In an open-ended tendon, one end of the tendon is tied to a driven pulley while the other end is attached to a linear actuator or a driving pulley that is installed on a rotary actuator. The driven pulley is usually attached to a link to be controlled. Figure 1(a) shows two pulleys, i and j, that are coupled by an open-ended tendon. Link k which is used to maintain a constant center distance for the two pulleys, is called the carrier. It is well known in the literature [11,12] that an n-DOF robotic mechanism requires at least (n+1) open-ended tendons to achieve a positive control.

In the endless tendon, each belt or tendon is wrapped around two or more pulleys of constant center distance in an endless loop. Figure 1(b) shows an endless tendon routed around two pulleys.

We note that both kinematic chains (or sub-chains) shown in Figs. 1(a) and 1(b) consist of three rigid links, links i, j and k, and a flexible ten-

don. The geometry of such mechanisms can be defined by the Denavit and Hartenberg's parameters [4], i.e. offset distance, twist angle between two joint axes, etc., in addition to the radii of the pulleys.

(b) Planar Schematic Representation. In this representation, we assign a positive direction of rotation to each joint axis in the mechanism of interest and consider the joint axis that is fixed to the reference frame as the first joint axis. Then, starting from the second joint axis, every axis is twisted about the common normal defined by the axis itself and its preceding axis until all the joint axes are parallel to each other and are pointed toward the same positive Z-direction. In this manner, the routing of tendons can be clearly shown without loosing the fundamental characteristics of relative rotation among the pulleys and their carriers.

Figures 2(a) and 2(b) show the planar schematics of the mechanisms shown in Figs. 1(a) and 1(b). The routing method shown in Fig. 2(a) is called the cross-type while the one shown in Fig. 2(b) is called the parallel-type. We note that the routing of the kinematic chain shown in Fig. 1(a) can also be sketched in a parallel-type construction if the definition of the positive Z-direction for either one of the two axes has been reversed. Although, this change does effect the sign of rotation in the fundamental circuit equation to be described below, it has no effect on the actual motion of the mechanism.

In general, two pulleys are said to have parallel-type routing if a positive rotation of one pulley, with respect to its carrier, produces a positive rotation of the other, and cross-type routing if a positive rotation of one pulley produces a negative rotation of the other.

(c) Graph Representation. In the graph representation, links are denoted by vertices and joints by edges. The edge connection between vertices corresponds to the joint connection between links. Every pair of pulleys coupled together by a tendon, either open-ended or endless tendon, is considered as a pulley pair. In this regard we have treated the tendon as an element which merely provides the necessary constraints to the two coupled pulleys. In order to distinguish different types of pair connections, turning pair is denoted by thin edge, parallel-type routing by double-line edge, and cross-type routing by heavy edge. Further, thin edges are labeled according to their axis locations. The graph of a tendon-driven articulated mechanism is, therefore, similar to that of an epicyclic gear train.

Figure 3(a) shows the graph representation for the tendon-driven mechanism shown in Fig. 2(a), where the vertices i, j and k correspond to links i, j, and k; thin edges i-k and j-k correspond to the turning pairs connecting links i and k, and links j and k; heavy edge i-j corresponds to the cross-type routing between links i and j; and the edge labels a and b corresponds to the axis levels a and b, respectively. Similarly, Fig. 3(b) shows the graph representation of the mechanism shown in Fig. 2(b) in which the parallel-type routing is denoted by a double-line edge.

4. Structural Characteristics

Similar to epicyclic gear trains, the graph of tendon-driven articulated mechanisms can be characterized by the following fundamental rules:

(i) For an n-link, F degrees of freedom, tendon-driven articulated mechanism, there are n-1 turning pairs and n-F-1 pulley pairs.

(ii) The subgraph obtained by deleting all the double-line and heavy edges is a tree, and there can be no circuit formed exclusively by thin edges.

(iii) Any double-line or heavy edge added to the tree forms a fundamental circuit (f-circuit) having one double-line or heavy edge and several thin edges.

(iv) The number of f-circuits equals the number of double-line and heavy edges.

(v) Each thin edge can be characterized by a level which identifies the axis location of a turning pair.

(vi) In each f-circuit there is one vertex, called the transfer vertex, such that all edges on one side of the transfer vertex are at the same level and edges on the opposite side are at a different level. The transfer vertex corresponds to the carrier in a pulley train.

5. Basic Equations

(a) Fundamental Circuit Equation. Let i and j denote the vertices of a pulley pair in an f-circuit for which k is the transfer vertex. Then, links i, j and k constitute a simple tendon-and-pulley train. We can assign a positive direction to each joint axis of the pulley pair, and write a fundamental circuit equation as shown below:

$$R_i \, \theta_{i,k} = \pm R_j \, \theta_{j,k} \qquad (1)$$

where $\theta_{i,k}$ and $\theta_{j,k}$ denote the relative rotations of links i and j with respect to link k, and, R_i and R_j denote the radii of the two matching pulleys, i and

j, respectively. The sign of Eq. (1) is to be determined by the routing of the tendon: positive for the parallel-type routing and negative for the cross-type. Note that Eq. (1) is valid whether the carrier is fixed or not.

(b) Coaxial Condition. Let i, j, and k be three links that share a common joint axis, then similar to epicyclic gear trains, the following chain rule applies:

$$\theta_{i,j} = \theta_{i,k} - \theta_{j,k} \tag{2}$$

Equation (2) is useful for relating the relative rotations among three or more coaxial links.

(c) Single-Tendon-Driven Pulley Trains. Let links 0, 1, 2 and 3 be connected in series, by turning pairs, to form a spatial open-loop chain; let a, b and c be the consecutive joint axes; and let pulleys j, j+1 and j+2 be pivoted about the joint axes a, b and c, respectively, as shown in Fig. 4(a). Pulleys j and j+1 are free to rotate with respect to links 0, 1, and 2 while pulley j+2 is rigidly tied to link 3. An endless tendon has been routed around these pulleys as shown in Fig. 4(a). We consider link "0" as the base link and link 3 as the link to be controlled, and seek to find a transformation between the rotation of the base pulley, j, and the joint angles, $\theta_{1,0}$, $\theta_{2,1}$ and $\theta_{3,2}$, in the open-loop chain.

Figure 4(b) shows the corresponding graph representation of Fig. 4(a). This graph consists of two f-circuits: (j, j+1, 1) and (j+1, 3, 2), where the first two numbers in the parenthesis denote the link numbers of a pulley pair, and the third denotes the corresponding carrier. Writing Eq. (1) once for each of the two f-circuits, we obtain:

$$R_j \theta_{j,1} = R_{j+1} \theta_{j+1,1} \tag{3}$$

and

$$R_{j+1} \theta_{j+1,2} = R_{j+2} \theta_{3,2} \tag{4}$$

Since links 0, 1 and j are coaxial, we have

$$\theta_{j,1} = \theta_{j,0} - \theta_{1,0} \tag{5}$$

Similarly, since links 1, 2 and j+1 are coaxial, we have

$$\theta_{j+1,2} = \theta_{j+1,1} - \theta_{2,1} \tag{6}$$

Substituting Eqs. (5) and (6) into (3) and (4) respectively, and then eliminating $\theta_{j+1,1}$ from the two resulting equations, we obtain:

$$\theta_{j,0} = \theta_{1,0} + (R_{j+1}/R_j)\theta_{2,1} + (R_{j+2}/R_j)\theta_{3,2} \tag{7}$$

Equation (7) provides the influence of the joint angles, $\theta_{1,0}$, $\theta_{2,1}$ and $\theta_{3,2}$, on the rotation of the base pulley, $\theta_{j,0}$. In general, we can write the relationship between the rotation of a base pulley and the joint angles in an open-loop chain with m+1 link as follows:

$$\theta_{j,0} = \theta_{1,0} \pm (R_{j+1}/R_j)\theta_{2,1} \pm (R_{j+2}/R_j)\theta_{3,2}$$

$$\pm \ldots . \pm (R_{j+m-1}/R_j)\theta_{m,m-1} \tag{8}$$

The sign of each term, $(R_{j+k-1}/R_j)\theta_{k,k-1}$, in Eq. (8) is to be determined by the number of cross-type routing preceding the kth joint axis. If the number of cross-type routing is even, then the sign is positive, otherwise it is

negative. This equation can be obtained by an inspection of the kinematic structure without going through the graph representation, once we become familiar with the subject.

Taking the derivative of Eq. (8), we obtain

$$d\theta_{j,0} = d\theta_{1,0} \pm (R_{j+1}/R_j)\, d\theta_{2,1} \pm (R_{j+2}/R_j)\, d\theta_{3,2}$$

$$\pm \ldots . \pm (R_{j+m-1}/R_j)\, d\theta_{m,m-1} \qquad (9)$$

where d( ) denotes the derivative of ( ). Hence, the coefficients of each derivative on the right-hand side of Eq. (9) may be considered as the partial rate of change of the base pulley rotation with respect to the corresponding joint angle.

6. Kinematics of Tendon-Driven Robotic Mechanisms

It has been shown in a previous paper that the graph of spatial robotic bevel-gear trains can be reconfigured into a canonical form from which an equivalent open-loop chain can be identified [16]. Similarly, we can also construct a canonical graph to represent the topological structure of a tendon-driven robotic mechanism, and identify the associated equivalent open-loop chain. Hence, the kinematic analysis of articulated, tendon-driven, robotic devices can be accomplished in two steps. First, the end-effector position and/or orientation can be related to the joint angles associated with the equivalent open-loop chain. Then, these joint angles can be related to the rotational displacements of the base pulleys.

In what follows, we describe a systematic procedure for the derivation of the linear transformation relating the rotational displacements of the base pulleys and the joint angles. Three examples will be used to illustrate the principle:

Example 1. Three-DOF Robotic Arm Driven by Endless Tendons.

Figure 5(a) shows the planar schematic of a spatial robotic arm. Pulleys 4 and 5 are free to rotate about axis "a," pulleys 2 and 6 are free to rotate about axis "b," and pulley 3 is free to rotate about axis "c." The first moving link serves as the carrier for the pulley pairs (4, 2), and (5, 6), the second moving link which is rigidly tied to pulley 2, serves as the carrier for the pulley pair (6, 3), and the third moving link is attached to pulley 3. The first tendon connects pulleys 4 and 2 and the second tendon connects pulleys 5, 6 and 3. Overall, the mechanism consists of seven rigid links and two endless tendons. It has three degrees of freedom. We can designate links 1, 4 and 5 as the inputs and link 3 as the output or end-effector. The mechanism shown in Fig. 5(a) has been sketched in its zero reference position [16].

Figure 5(b) shows the corresponding canonical graph of the mechanism. It can be seen from Figure 5(b) that the equivalent open-loop chain for the mechanism consists of links 0-1-2-3, and there are three f-circuits: (2, 4, 1), (5, 6, 1) and (3, 6, 2). Figure 5(c) shows the routing of the two tendons with respect to the equivalent open-loop chain. The parallel-type routing is clearly depicted in both Figures 5(b) and 5(c).

Writing Eq. (8) once for each of the two tendon routings shown in Fig. 5(c), we obtain,

$$\theta_{4,0} = \theta_{1,0} + (R_2/R_4)\theta_{2,1} \tag{10}$$

and

$$\theta_{5,0} = \theta_{1,0} + (R_6/R_5)\theta_{2,1} + (R_3/R_5)\theta_{3,2} \tag{11}$$

where R_j, $j = 2, 3, 4, \ldots$, denote the radii of the pulleys shown in Fig. 5(a).

We can add an identity equation, $\theta_{1,0} = \theta_{1,0}$, to Eqs. (10) and (11) and then rearrange them in a matrix form as shown below:

$$\begin{bmatrix} \theta_{1,0} \\ \theta_{4,0} \\ \theta_{5,0} \end{bmatrix} = \begin{bmatrix} 1 & 0 & 0 \\ 1 & R_2/R_4 & 0 \\ 1 & R_6/R_5 & R_3/R_5 \end{bmatrix} \begin{bmatrix} \theta_{1,0} \\ \theta_{2,1} \\ \theta_{3,2} \end{bmatrix} \tag{12}$$

Equation (12) provides the necessary transformation between the angular displacements of the input links ($\theta_{1,0}$, $\theta_{4,0}$ and $\theta_{5,0}$) and the joint angles ($\theta_{1,0}$, $\theta_{2,1}$ and $\theta_{3,2}$). The equations are linear and its inverse transformation can be easily derived.

Let $R_4 = R_2$ and $R_5 = R_6 = R_3$, then Eq. (12) becomes,

$$\begin{bmatrix} \theta_{1,0} \\ \theta_{4,0} \\ \theta_{5,0} \end{bmatrix} = \begin{bmatrix} 1 & 0 & 0 \\ 1 & 1 & 0 \\ 1 & 1 & 1 \end{bmatrix} \begin{bmatrix} \theta_{1,0} \\ \theta_{2,1} \\ \theta_{3,2} \end{bmatrix} \tag{13}$$

and its inverse transformation is given by,

$$\begin{bmatrix} \theta_{1,0} \\ \theta_{2,1} \\ \theta_{3,2} \end{bmatrix} = \begin{bmatrix} 1 & 0 & 0 \\ -1 & 1 & 0 \\ 0 & -1 & 1 \end{bmatrix} \begin{bmatrix} \theta_{1,0} \\ \theta_{4,0} \\ \theta_{5,0} \end{bmatrix} \tag{14}$$

We note that, for this special proportion, the second joint is locked when links 1 and 4 are driven at the same rate; the third joint is locked when links 4 and 5 are driven at the same rate; and both the second and third joints are locked when links 1, 4 and 5 are all driven at the same rate.

Example 2. The Stanford/JPL Finger.

Figure 6(a) shows the functional representation of the Stanford/JPL Finger taken from [10], where the first joint axis, Z_1, is fixed to the base link, link 0; the second joint axis, Z_2, is perpendicular to the first; and the third joint axis, Z_3, is parallel to the second. Pulleys 4, 5, 6 and 7 are free to rotate about the first joint axis, pulleys 2 and 8 are free to rotate about the second joint axis, and pulley 3 is free to rotate about the third joint axis. The first link, link 1, serves as the carrier for the pulley pairs (4, 2), (5, 2), (6, 8), and (7, 8). The second link, which is attached to pulley 2, serves as the carrier for the pulley pair (8, 3). The third link is attached to pulley 3. The first tendon connects pulley 2 to 4, the second connects pulley 2 to 5, the third connects pulley 3 to 8 and then 6, and the fourth connects pulley 3 to 8 and then 7 in open-ended routing as shown in

Figure 6(a). Over all, the mechanism consists of nine rigid links and four unidirectional tendons. Although it has three degrees of freedom, it requires four open-ended tendons to achieve positive control of the mechanism.

Figure 6(b) shows the mechanism in a planar schematic. The equivalent open-loop chain consists of links 0-1-2-3. The routing of the four tendons with respect to the equivalent open-loop chain is clearly depicted in Fig. 6(b).

Writing Eq. (8) once for each of the four tendon routings shown in Fig. 6(b), we obtain:

$$\theta_{4,0} = \theta_{1,0} + (R_2/R_4)\theta_{2,1} \tag{15}$$

$$\theta_{5,0} = \theta_{1,0} - (R_2/R_5)\theta_{2,1} \tag{16}$$

$$\theta_{6,0} = \theta_{1,0} - (R_8/R_6)\theta_{2,1} - (R_3/R_6)\theta_{3,2} \tag{17}$$

and

$$\theta_{7,0} = \theta_{1,0} + (R_8/R_7)\theta_{2,1} + (R_3/R_7)\theta_{3,2} \tag{18}$$

Writing Eqs. (15)-(18) in matrix form, we obtain:

$$\begin{bmatrix} \theta_{4,0} \\ \theta_{5,0} \\ \theta_{6,0} \\ \theta_{7,0} \end{bmatrix} = \begin{bmatrix} 1 & R_2/R_4 & 0 \\ 1 & -R_2/R_5 & 0 \\ 1 & -R_8/R_6 & -R_3/R_6 \\ 1 & R_8/R_7 & R_3/R_7 \end{bmatrix} \begin{bmatrix} \theta_{1,0} \\ \theta_{2,1} \\ \theta_{3,2} \end{bmatrix} \tag{19}$$

The linear displacements of the tendons to be pulled away from their neutral positions are given by:

$$s_4 = R_4\theta_{4,0} \tag{20}$$

$$s_5 = R_5\theta_{5,0} \tag{21}$$

$$s_6 = -R_6\theta_{6,0} \tag{22}$$

and

$$s_7 = -R_7\theta_{7,0} \tag{23}$$

Multiplying the first row of Eq. (19) by R_4, the second row by R_5, the third row by $-R_6$, and the fourth row by $-R_7$, we obtain,

$$\bar{s} = A\,\bar{\theta} \tag{24}$$

where $\bar{s} = (s_4, s_5, s_6, s_7)^T$, $\bar{\theta} = (\theta_{1,0}, \theta_{2,1}, \theta_{3,2})^T$, and

$$A = \begin{bmatrix} R_4 & R_2 & 0 \\ R_5 & -R_2 & 0 \\ -R_6 & R_8 & R_3 \\ -R_7 & -R_8 & -R_3 \end{bmatrix} \tag{25}$$

where the superscript T denotes the transpose of the associated matrix.

We note that if $R_4 = R_5 = R_6 = R_7$, and $R_2 = R_8$, then the matrix A can be decomposed into the product of two matrices:

$$A = B\,R \tag{26}$$

where

$$B = \begin{bmatrix} 1 & 1 & 0 \\ 1 & -1 & 0 \\ -1 & 1 & 1 \\ -1 & -1 & -1 \end{bmatrix} \tag{27}$$

and

$$R = \begin{bmatrix} R_4 & 0 & 0 \\ 0 & R_2 & 0 \\ 0 & 0 & R_3 \end{bmatrix} \tag{28}$$

Matrix B which depends on the routing of tendons, is called the structure matrix. Matrix R, under the assumption that all pulleys on the same joint axis are of the same size, is a diagonal matrix whose non-zero elements are the radii of the pulleys installed at the consecutive axes of the equivalent open-loop chain.

We conclude that, once the joint angles, $\theta_{1,0}$, $\theta_{2,1}$ and $\theta_{3,2}$ are known, linear displacements of the tendons can be uniquely determined. On the other hand, we cannot specify all the four linear displacements, s_1, s_2, s_3, and s_4 arbitrarily. Once three of the four linear displacements are specified, the fourth linear displacement and the joint angles are to be determined by Eq. (24).

It can be shown that the vector of forces, $\bar{f}$, exerted by the tendons are related to the torques, $\bar{\tau}$, in the joints of the open-loop chain by the following relationship:

$$\bar{\tau} = A^T \bar{f} \tag{29}$$

where $\bar{\tau} = (\tau_{1,0}, \tau_{2,1}, \tau_{3,2})^T$, and $\bar{f} = (f_4, f_5, f_6, f_7)^T$.

Hence, once tensions in the tendons are specified, torques in the joints can be uniquely determined. On the other hand, when torques in the joints are specified, tensions in the tendons are indeterminate. For a given set of joint torques, Eq. (29) yields three linear equations in four unknowns. The homogeneous solution corresponds to a set of tensions that result in no joint torque about any of the three axes. The general solution is given by the sum of a particular solution plus the homogeneous solution multiplied by an arbitrary constant. Thus positive tension can be maintained by selecting an appropriate multiplier to the homogeneous solution.

Example 3. A Six DOF Manipulator.

We now consider a general six DOF manipulator as shown in Fig. 7 in a planar schematic. For the reason of clarity, we have sketched each individual routing of the tendons about the equivalent open-loop chain on a separate drawing. The equivalent open-loop chains is made up of links 0-1-2-3-4-5-6. It can be seen from Fig. 7 that there are twenty pulleys and five endless tendons. Pulleys 2 to 6 are rigidly attached to links 2 to 6, respectively. Over all there are twenty-two rigid links, twenty-one turning pairs and fifteen pulley pairs. Hence, the mechanism has six degrees of freedom. We can designate pulleys 7 to 11 and the first moving link as the input links and seek for the transformation between the rotational displacements of these inputs and the joint angles associated with the equivalent open-loop chain.

Writing Eq. (8) once for each of the tendon routing shown in Fig. 7, we obtain the following linear transformation in matrix form:

$$\bar{\phi} = A\,\bar{\theta} \tag{30}$$

where $\bar{\phi} = (\theta_{1,0}, \theta_{7,0}, \theta_{8,0}, \theta_{9,0}, \theta_{10,0}, \theta_{11,0})^T$

$$\bar{\theta} = (\theta_{1,0}, \theta_{2,1}, \theta_{3,2}, \theta_{4,3}, \theta_{5,4}, \theta_{6,5})^T$$

and

$$A = \begin{bmatrix} 1 & 0 & 0 & 0 & 0 & 0 \\ 1 & R_2/R_7 & 0 & 0 & 0 & 0 \\ 1 & R_{12}/R_8 & R_3/R_8 & 0 & 0 & 0 \\ 1 & R_{13}/R_9 & R_{16}/R_9 & R_4/R_9 & 0 & 0 \\ 1 & R_{14}/R_{10} & R_{17}/R_{10} & -R_{19}/R_{10} & -R_5/R_{10} & 0 \\ 1 & R_{15}/R_{11} & -R_{18}/R_{11} & -R_{20}/R_{11} & -R_{21}/R_{11} & R_6/R_{11} \end{bmatrix} \quad (31)$$

Again, Let $R_7 = R_8 = R_9 = R_{10} = R_{11}$, $R_2 = R_{12} = R_{13} = R_{14} = R_{15}$, $R_3 = R_{16} = R_{17} = R_{18}$, $R_4 = R_{19} = R_{20}$, and $R_5 = R_{21}$, then the matrix A can be decomposed into the product of two matrices as shown below:

$$A = B\ R \quad (32)$$

where

$$B = \begin{bmatrix} 1 & 0 & 0 & 0 & 0 & 0 \\ 1 & 1 & 0 & 0 & 0 & 0 \\ 1 & 1 & 1 & 0 & 0 & 0 \\ 1 & 1 & 1 & 1 & 0 & 0 \\ 1 & 1 & 1 & -1 & -1 & 0 \\ 1 & 1 & -1 & -1 & -1 & 1 \end{bmatrix}$$

and,

$$R = \begin{bmatrix} 1 & 0 & 0 & 0 & 0 & 0 \\ 0 & R_2/R_7 & 0 & 0 & 0 & 0 \\ 0 & 0 & R_3/R_8 & 0 & 0 & 0 \\ 0 & 0 & 0 & R_4/R_9 & 0 & 0 \\ 0 & 0 & 0 & 0 & R_5/R_{10} & 0 \\ 0 & 0 & 0 & 0 & 0 & R_6/R_{11} \end{bmatrix}$$

The matrix B is called the structure matrix and matrix R the radius matrix. This example illustrates how easily we can derive the matrix of transformation by merely inspecting the kinematic structure of the mechanism.

7. Conclusions

The kinematic structure of tendon-driven robotic mechanisms has been investigated with the aid of graph theory. The correspondence between the graph representation of the kinematic structure and the mechanism has been established. We have shown that the routing of tendons in a spatial robotic device can be best represented by the planar schematic. We have also shown that the kinematic structure of tendon-driven robotic mechanisms is similar to that of epicyclic gear trains.

Using the concept of fundamental circuit, a general expression relating the rotational displacement of a base pulley to the joint angles of a single-tendon-driven mechanism has been derived. We have shown that displacement equations of a tendon-driven robotic mechanism can be easily obtained by an inspection of the kinematic structure of the mechanism. The theory has been demonstrated by the kinematic analysis of three articulated robotic devices.

8. Acknowledgement

The authors wish to thank the Systems Research Center of the University of Maryland for the support of this research through an NSF grant No. NSF-CDR-8500108. The authors also wish to thank Professor F. Freudenstein of Columbia University for suggesting the study of this subject.

9. References

1. Buchsbaum, F., 1968, "Structural Classification and Type Synthesis of Mechanisms with Multiple Elements," Eng. ScD Dissertation, Columbia University, Publication 67-15479, University Microfilm, Inc., Ann Arbor, MI.

2. Buchsbaum, F. and Freudenstein, F., 1970, "Synthesis of Kinematic Structure of Geared Kinematic Chains and Other Mechanisms," Journal of Mechanisms, Vol. 5, pp. 357-392.

3. Day, C.P., Akeel, H.,A., and Gutkowski, L.J., Sept. 1983, "Kinematic Design and Analysis of Coupled Planetary Bevel-Gear Trains" ASME Journal of Mechanisms, Transmissions, and Automation in Design, Vol. 105, No. 3, pp. 441-445.

4. Denavit, J., and Hartenberg, R.S., 1955, "A Kinematic Notation for Lower Pair Mechanisms Based on Matrices," ASME Journal of Applied Mechanics, Vol. 77, pp. 215-211.

5. Freudenstein, F., Feb. 1971, "An Application of Boolean Algebra to the Motion of Epicyclic Drives," ASME Journal of Engineering of Industry, Vol. 93, Series B, pp. 176-182.

6. Freudenstein, F., Longman, R.W. and Chen, C.K., Sept. 1984, "Kinematic Analysis of Robotic Bevel-Gear Trains," ASME Journal of Mechanisms, Transmissions, and Automation in Design, Vol. 106, No. 3, pp. 371-375.

7. Freudenstein, F., and Yang, A.T., 1972, "Kinematics and Statics of a Coupled Epicyclic Spur-Gear Train," Journal of Mechanisms and Machine Theory, Vol. 7, pp. 263-275.

8. Jacobsen, S.C., Wood, J.E., Knutti, D.F., and Biggers, K.B., "The Utah/MIT Dextrous Hand: Work in Progress," The International Journal of Robotics Research, Vol. 3, No. 4, pp. 21-50.

9. Leaver, S.O., and McCarthy, J.M., 1987, "The Design of Three Jointed Two-Degree-of-Freedom Robot Fingers," ASME Advances in Design Automation, Volume Two: Robotics, Mechanisms, and Machine System - DE-Vol. 10-2, pp. 127-134.

10. Mason, M.T., and Salisbury, J.K. Jr., 1985, Robot Hands and the Mechanics of Manipulation, The MIT Press, Cambridge, Mass.

11. Morecki, A., Ekiel, J., and Fidelus, K., 1984, Cybernatic Systems of Limb Movements in Man, Animals and Robots, PWN-Polish Scientific Publishers, Ellis Horwood Limited, Warszawa, Poland.

12. Morecki, A., et al., March 1980, "Synthesis and Control of the Anthropomorphic Two-Handed Manipulator," Proceedings of the 10th Inter. Symposium on Industrial Robots, Milan, Italy, pp. 461-474.

13. Pham, D.T., and Heginbotham, W.B., 1986, Robot Grippers, Springer-Verlag, IFS (Publications) Ltd, UK.

14. Stackhouse, T., 1979, "A New Concept in Wrist Flexibility," Proceedings of the 9th Inter. Symposium on Industrial Robots, Washington, D.C., pp. 589-599.

15. Tsai, L.W., 1985, "An Algorithm for the Kinematic Analysis of Epicyclic Gear Trains," Proceedings of the 9th Applied Mechanisms Conference, Kansas City, Missouri.

16. Tsai, L.W., 1987, "The Kinematics of Robotic Bevel-Gear Trains," Proceedings of the 1987 IEEE Inter. Conference on Robotics and Automation, Raleigh, N. Carolina. Also accepted for Publication in the IEEE Journal of Robotics and Automation.

Figure Captions

Figure 1. Two Basic Tendon-Routing Methods.

Figure 2. Planar Schematic Representation of Tendon-Driven Mechanisms.

Figure 3. Graph Representation of Tendon-Driven Mechanisms.

Figure 4. A Single-Tendon-DrivenArticulated Mechanism.

Figure 5. A Three-DOF Robotic Arm Driven by Endless Tendons.

Figure 6. The Stanford/JPL Finger.

Figure 7. A Six DOF Manipulator-Planar Schematic.

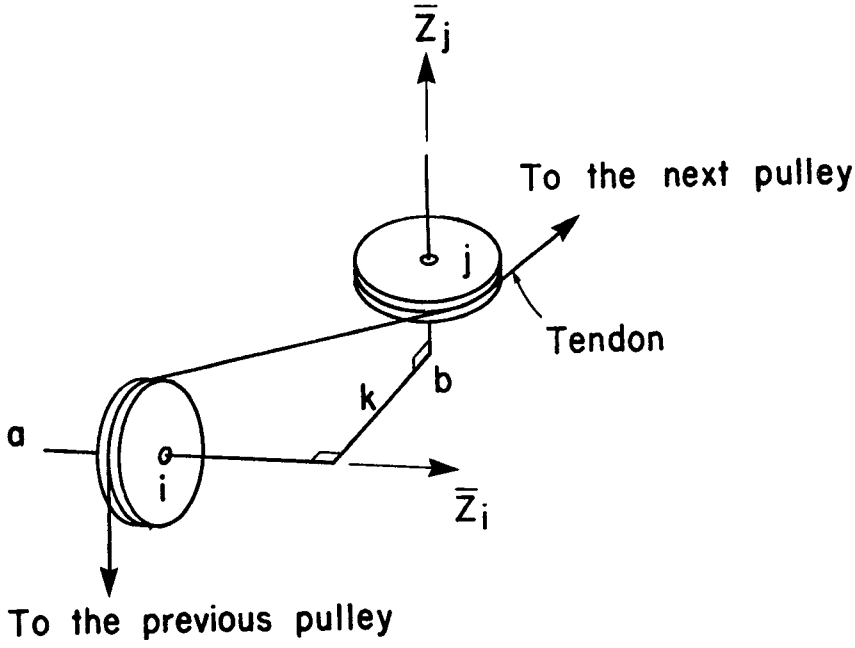

Figure 1(a) Open - Ended Tendon

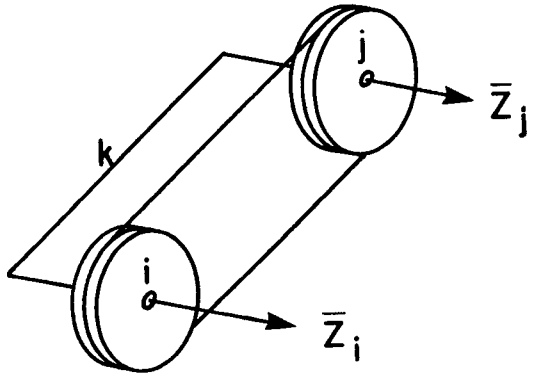

Figure 1(b) Endless Tendon

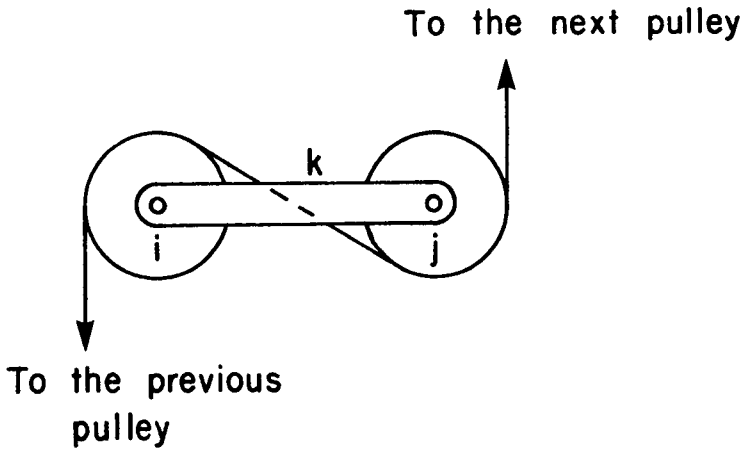

Figure 2 (a) Planar Schematic
of Figure 1 (a)

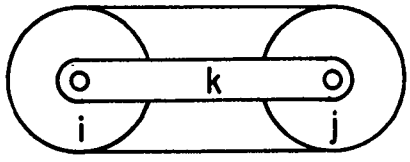

Figure 2 (b) Planar Schematic
of Figure 1 (b)

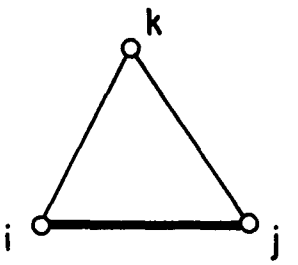

Figure 3 (a) Graph Representation of Figure 2 (a)

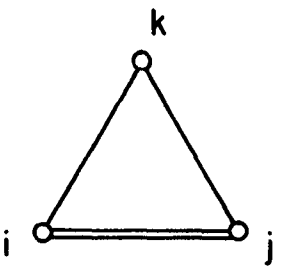

Figure 3 (b) Graph Representation of Figure 2 (b)

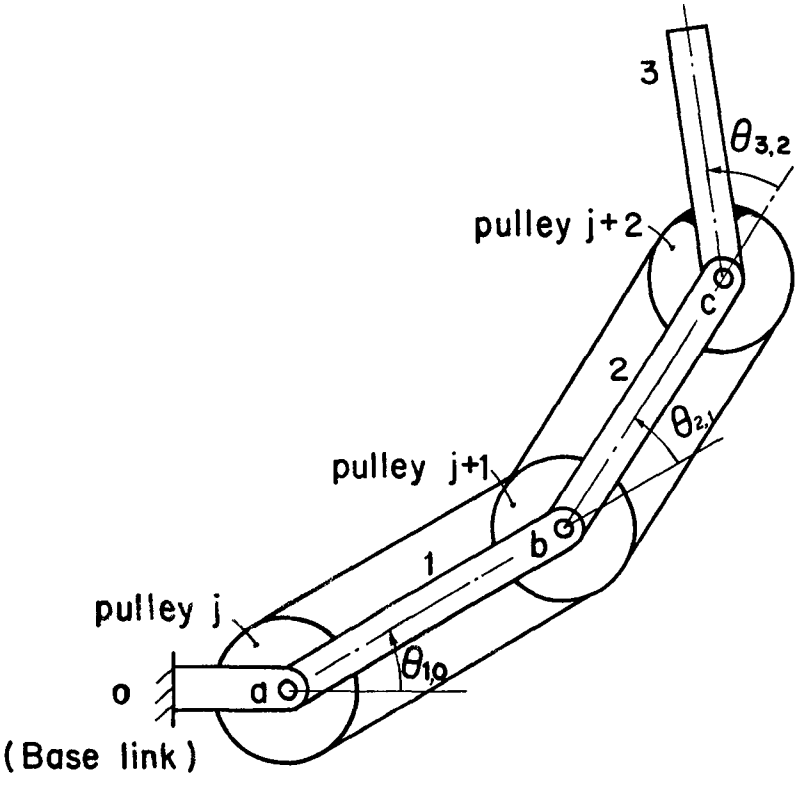

Figure 4(a) A Single Tendon-Driven Articulated Mechanism

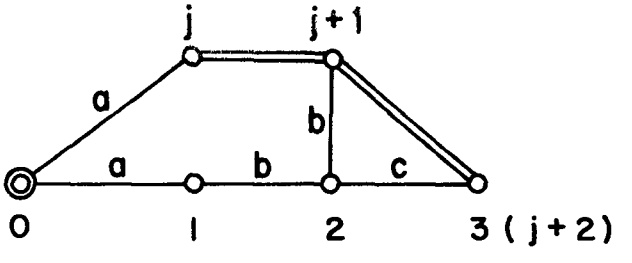

Figure 4(b) Graph Representation of Figure 4(a)

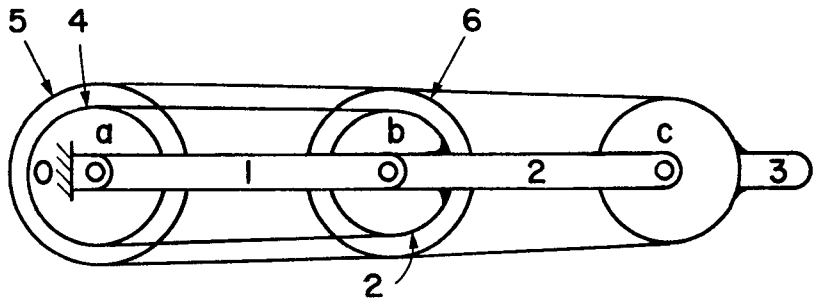

Figure 5(a) Planar Schematic Representation of a Three DOF Manipulator

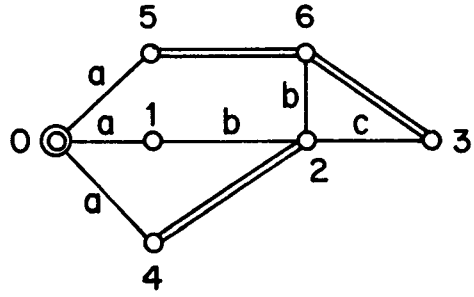

Figure 5(b) Canonical Graph of Figure 5(a)

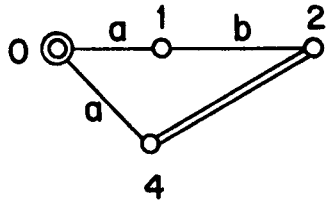

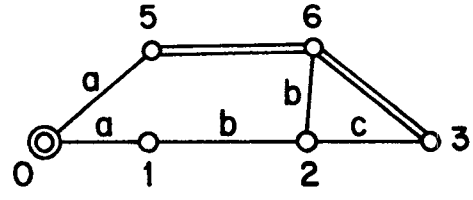

Figure 5(c) Two Tendon Drives

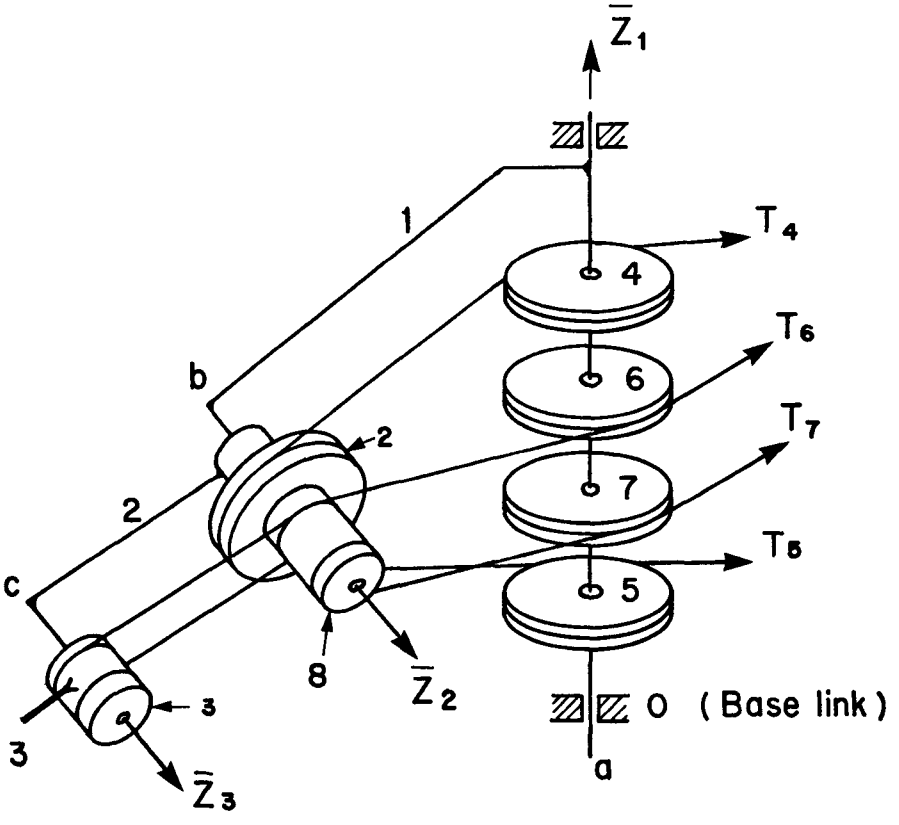

Figure 6(a) Functional Representation of Stanford/JPL Finger

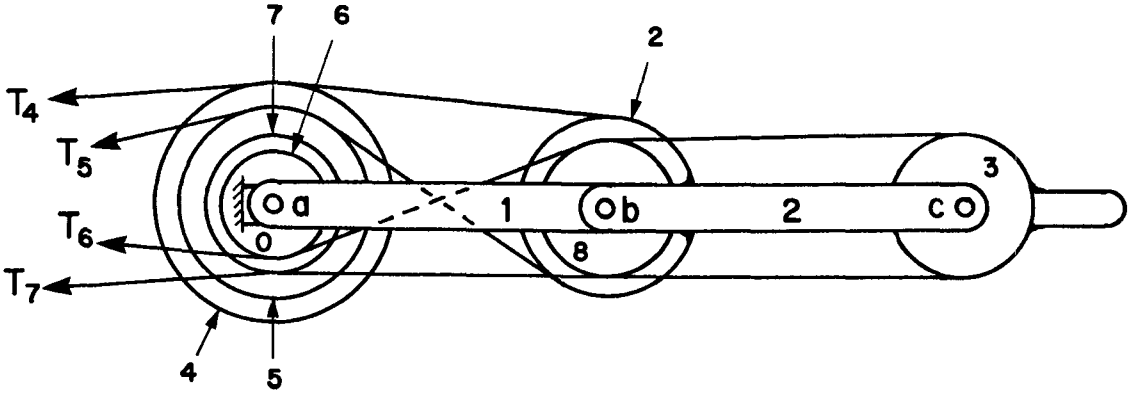

Figure 6(b) Planar Schematic of Figure 6(a)

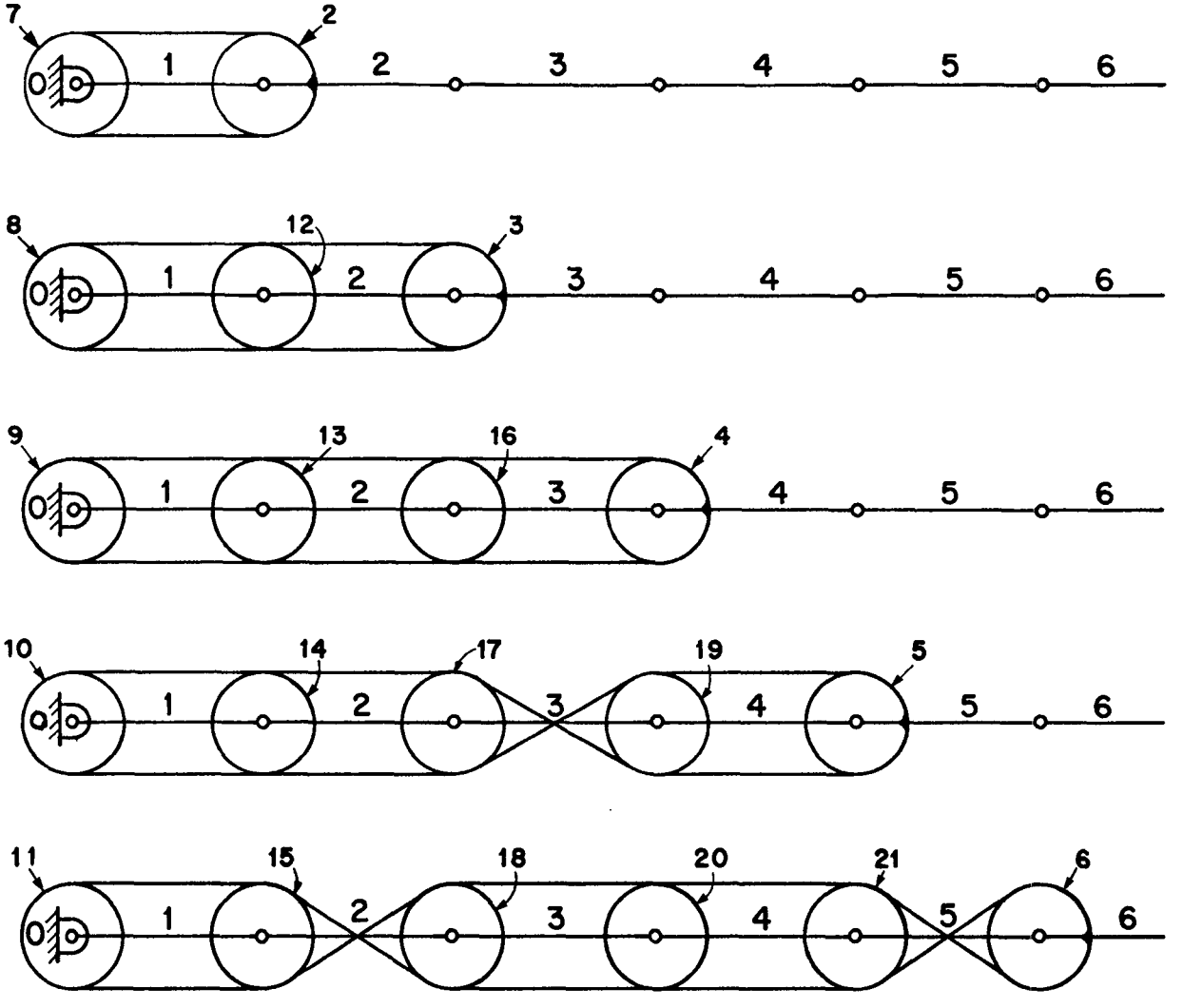

Figure 7 A Six DOF Manipulator–Planar Schematic